Oxidation of DNA Hairpins by Oxoruthenium(IV): Effects of Sterics and Secondary Structure

Pamela J. Carter, C.-C. Cheng, and H. Holden Thorp*

Department of Chemistry, University of North Carolina at Chapel Hill, Chapel Hill, North Carolina 27599-3290

Received December 6, 1995[⊗]

The effects of steric hindrance on the oxidation of DNA by polypyridyl oxoruthenium(IV) complexes have been investigated. The complexes oxidize DNA by activation either of the 1′ ribose C−H bond or by oxo transfer to the guanine nucleobase. A method is presented for determining the relative rates of activation of individual sites from the dependence of the extent of cleavage on the oxidant concentration. This analysis shows that hybridization of the labeled strand to its complement attenuates the rate of oxidation of guanine more effectively than the rate of sugar oxidation. Accordingly, higher ratios of guanine/sugar oxidation are observed in single strands. Among the individual guanine residues, however, the relative reactivities are not altered by hybridization; a similar result is obtained for sugar oxidation. This result implies that sequence-dependent chemical reactivity is partly responsible for the different extents of cleavage observed within the sequence. The ability of hybridization to protect guanine from oxidation is also apparent in hairpin studies, where the stem guanines are much less reactive than the loop guanines, and altered sugar conformations in the loop lead to modulated reactivity. Finally, a set of sterically differentiated complexes shows greater steric effects for oxidation of guanine compared to oxidation of sugar, as expected from the relative rates of the single strand and duplexes.

An understanding of the distribution of cleavage sites for oxidation of a complex nucleic acid by a small molecule requires a knowledge of the rate-determining step in the cleavage mechanism. Attempts to understand DNA cleavage within a kinetic context have been applied to iron bleomycin (FeBLM),[1−3] enediyne antibiotics,[4−7] and oxoruthenium(IV) complexes $Ru^{IV}O^{2+}$.[8−10] For FeBLM, the formation of activated bleomycin involves reduction and O_2 activation, and the precise steps of the mechanism are still a subject of investigation.[11−14] For the enediynes, thiol-activated Bergman cyclization is required to form the active benzene diradical that cleaves DNA.[5−7] Related considerations apply to the Mn−porphryin/$KHSO_5$ system.[15] Determining which intermediate in the activation process is responsible for the cleavage pattern in these systems therefore becomes a complicating factor in understanding the cleavage mechanism. In the $Ru^{IV}O^{2+}$ system, the complex is prepared and added to DNA in the activated form and therefore follows the simplest mechanism, where binding of the activated cleavage agent to a given site precedes oxidation of the site:

$$Ru^{IV}O^{2+} + DNA \rightleftharpoons Ru^{IV}O^{2+}\cdot DNA \rightarrow Ru^{II}OH_2{}^{2+}\cdot DNA_{ox} \quad (1)$$

In the "parlance of the enzymologist",[1] an analogy to enzyme kinetics can be drawn, with the "commitment to catalysis" of the cleavage agent analogous to the fraction of binding events that lead to cleavage. Investigations along these lines are particularly appropriate for $Ru^{IV}O^{2+}$ because the precise concentration of the active oxidant is known and the kinetics of metal reduction can be followed using optical spectroscopy.[16,17]

The complex $Ru(tpy)(bpy)O^{2+}$ cleaves DNA by oxidation of the 1′ position of deoxyribose to yield frank scission that is enhanced by piperdine treatment and by oxidation of guanine bases to yield only piperidine-labile scission.[8] The complex binds to double-stranded DNA electrostatically,[18] which produces a pre-steady-state "burst" phase in kinetics traces where the initially bound $Ru^{IV}O^{2+}$ is reduced prior to establishment of the binding equilibrium.[10] The complex $Ru(tpy)(dppz)O^{2+}$ exhibits the same cleavage reactivity as the bpy complex but binds via an intercalative mode that both unwinds and lengthens DNA.[10] The binding thermodynamics comprise contributions from the same electrostatic component seen for the bpy complex (2.5 kcal/mol at 75 mM Na^+) and an intercalative component equal to that for ethidium bromide (6 kcal/mol).[19] As a result

[⊗] Abstract published in *Advance ACS Abstracts,* May 1, 1996.

(1) Worth, L., Jr.; Frank, B. L.; Christner, D. F.; Absalon, M. J.; Stubbe, J.; Kozarich, J. W. *Biochemistry* **1993**, *32*, 2601.
(2) Kozarich, J. W.; Worth, L., Jr.; Frank, B. L.; Christner, D. F.; Vanderwall, D. E.; Stubbe, J. *Science* **1989**, *245*, 1396.
(3) Hecht, S. M. *Bioconjugate Chem.* **1994**, *5*, 513−526.
(4) Frank, B. L.; Worth, L.; Christner, D. F.; Kozarich, J. W.; Stubbe, J.; Kappen, L. S.; Goldberg, I. H. *J. Am. Chem. Soc.* **1991**, *113*, 2271−2275.
(5) Myers, A. G.; Cohen, S. B.; Kwon, B. M. *J. Am. Chem. Soc.* **1994**, *116*, 1670−1682.
(6) Myers, A. G.; Cohen, S. B.; Kwon, B. M. *J. Am. Chem. Soc.* **1994**, *116*, 1255−1271.
(7) Chatterjee, M.; Mah, S. C.; Tullius, T. D.; Townsend, C. A. *J. Am. Chem. Soc.* **1995**, *117*, 8074−8082.
(8) Cheng, C.-C.; Goll, J. G.; Neyhart, G. A.; Welch, T. W.; Singh, P.; Thorp, H. H. *J. Am. Chem. Soc.* **1995**, *117*, 2970−2980.
(9) Neyhart, G. A.; Cheng, C.-C.; Thorp, H. H. *J. Am. Chem. Soc.* **1995**, *117*, 1463−1471.
(10) Neyhart, G. A.; Grover, N.; Smith, S. R.; Kalsbeck, W. A.; Fairley, T. A.; Cory, M.; Thorp, H. H. *J. Am. Chem. Soc.* **1993**, *115*, 4423.
(11) Guajardo, R. J.; Hudson, S. E.; Brown, S. J.; Mascharak, P. K. *J. Am. Chem. Soc.* **1993**, *115*, 7971−7977.
(12) Sam, J. W.; Tang, X.-J.; Peisach, J. *J. Am. Chem. Soc.* **1994**, *116*, 5250−5256.
(13) Sam, J. W.; Tang, X.-J.; Mogliozzo, R. S.; Peisach, J. *J. Am. Chem. Soc.* **1995**, *117*, 1012−1018.
(14) Westre, T. E.; Loeb, K. E.; Zaleski, J. M.; Hedman, B.; Hodgson, K. O.; Solomon, E. I. *J. Am. Chem. Soc.* **1995**, *117*, 1309−1313.
(15) Pitié, M.; Bernadou, J.; Meunier, B. *J. Am. Chem. Soc.* **1995**, *117*, 2935−2936.
(16) Neyhart, G. A.; Kalsbeck, W. A.; Welch, T. W.; Grover, N.; Thorp, H. H. *Adv. Chem. Ser.* **1995**, *246*, 405−430.
(17) Thorp, H. H. *Adv. Inorg. Chem.* **1995**, *43*, 127−177.
(18) Kalsbeck, W. A.; Thorp, H. H. *Inorg. Chem.* **1994**, *33*, 3427−3429.
(19) Kalsbeck, W. A.; Thorp, H. H. *J. Am. Chem. Soc.* **1993**, *115*, 7146−7151.

S0020-1669(95)01551-5 CCC: $12.00

of the tighter binding equilbrium, a greater fraction of the complex is reduced during the pre-steady-state phase of the cleavage reaction than with the bpy complex,[10] consistent with the enzyme analogy and eq 1.

Our goal is to understand at a quantitative level why some nucleotides in polymers of different structures and sequences are more reactive than others toward a particular cleavage agent. Most cleavage agents that bind DNA exhibit some variability in the extent of cleavage at different sites in the polymer.[16,17,20−23] For instance, the isotope effect for 4′ C−H bond activation by bleomycin varies from nucleotide to nucleotide within a DNA sequence.[2] A number of factors could lead to these observations, such as changes in the structure of the transition state, differences in the innate reactivity of the site, or variations in the competing rates of dissociation or self-inactivation.[1] Many other cleavage agents have been investigated in other laboratories[24−28] and, with the exception of $Fe(EDTA)^{2-}$ and $Pt_2(pop)_4^{4-}$ ($pop = P_2O_5H_2^{2-}$),[29,30] exhibit some dependence of cleavage intensity on the DNA sequence, which is pronounced in many cases. In many of these studies, sequence or structural specificity is ascribed to specificity in the binding of the metal complex to the biopolymer.[25,27] In the case of $Ru(tpy)(bpy)O^{2+}$ and related complexes discussed here, the binding equilibrium is primarily electrostatic,[18] which is generally nonspecific. An interesting exception are Ni macrocyclic complexes, which cleave guanine residues as a function of solvent accessibility.[31] The initial step in the reaction of these complexes is thought to involve covalent binding to the macromolecule, which is controlled by the solvent accessibility of the guanine N7.[31] This case is quite relevant to the discussion here except that the binding and cleavage reactions are decoupled in the Ni macrocycle case whereas here there is an intimate interplay described in detail below.

We have reported the relative rates of the base and sugar oxidation pathways during DNA cleavage by $Ru^{IV}O^{2+}$.[9] From densitometry and product analysis, the effective rate of guanine oxidation in single-stranded DNA is about 7 times faster than that of the sugar oxidation pathway. This rate difference was confirmed by detailed kinetics experiments on mononucleotides, which gave the same ratio. Stopped-flow kinetics studies on oxidation of GMP by $Ru(tpy)(bpy)O^{2+}$ show that the oxidation process involves an inner-sphere Ru−O−GMP covalent adduct. Sugar oxidation likely occurs via an outer-sphere hydrogen abstraction and is therefore less sterically demanding. We report here the exploitation of this idea in designing sterically hindered $Ru^{IV}O^{2+}$ complexes that exhibit a lower ratio of guanine to sugar oxidation.

Materials and Methods

Metal Complexes. The complexes $[Ru(tpy)(bpy)OH_2](ClO_4)_2$ and $[Ru(bpy)_2(py)(OH_2)](ClO_4)_2$ were prepared according to published procedures.[32,33] The complex *cis*-$[Ru(bpy)_2(OH_2)_2]^{2+}$ was prepared by dissolving $Ru(bpy)_2CO_3$[34] in distilled water using a dark container to prevent isomerization to the *trans* form. The oxidized metal complexes were prepared by electrochemical oxidation of the corresponding aquaruthenium(II) complexes in 10 mM sodium phosphate buffer (pH 7.0), as described previously.[10] The applied potentials were 1.0 V for both *cis*-$[Ru(bpy)_2(OH_2)_2]^{2+}$ and *cis*-$[Ru(bpy)_2(py)OH_2]^{2+}$ and 0.85 V for $[Ru(tpy)(bpy)OH_2]^{2+}$ (all potentials versus SSCE). Bulk electrolysis was continued until the current reached 8% of the initial value.

DNA Purification. The synthetic oligonucleotides were obtained from the Oligonucleotide Synthesis Center in the Department of Pathology at UNC. Further purification of the DNA samples was performed using HPLC, with a 15 cm column packed with Self Pack Poros 20 R2 (Perseptive Biosystems). A linear gradient of 0−10% was used (buffer A, 5% acetonitrile, 50 mM triethylammonium acetate; buffer B, 100% acetonitrile). The collected DNA solution was lyophilized to dryness, suspended in 1.5 M sodium acetate (60 μL) and precipitated twice with ethanol. The pellets were lyophilized to dryness and dissolved in MilliQ water. The oligomer concentrations were determined from the absorbance at 260 nm and are in terms of nucleotide phosphate.[35]

A small portion of the oligonucleotide solution was purified further and used for 5′-^{32}P-labeling. The DNA was run on a 20% polyacrylamide denaturing gel (750 V, 2.5 h). The DNA was visualized by UV-shadowing (254 nm) with the gel placed on top of a TLC F_{254} sheet. The DNA samples were carefully spliced from the gel. The gel pieces were crushed and soaked in MilliQ water, shaken for 2 h, and filtered to remove the acrylamide using a micropure 0.45 M separator (Amicon). The DNA concentration was determined from the absorbance at 260 nm, as described above.

DNA Reactions. The 5′-^{32}P-labeled oligomers were prepared by using T4 polynucleotide kinase and deoxyadenosine 5′-[γ-^{32}P]-triphosphate (Amersham). The ^{32}P-labeled DNA was isolated by ultracentrifugation (0−5 °C, 45 min) using Centricon-10 (Amicon). The filter was then washed with 1 mL of distilled water, followed by additional centrifugation (35 min). The extent of labeling was determined using a scintillation counter.

Oligonucleotides were annealed in 10 mM sodium phosphate buffer at pH 7.0 by heating to 90 °C for 5 min and cooled slowly (2−3 h) to 4 °C to ensure hairpin formation, which was then detected by running a native 20% polyacrylamide gel (acrylamide−bis(acrylamide) = 19:1) at 4 °C to prevent any thermal denaturation. The d[5′-TTCAA-**CAGTGT**TTGAA] hairpin exhibited a T_m of 37 °C as determined by optical spectrophotometry. In the case of the oligonucleotide d[5′-CGCG**TTGTT**CGCG], formation of a dimer was not observed.

The DNA cleavage reactions were performed in 10 mM sodium phosphate buffer (pH 7.0) with a final DNA concentration of 5 μM and ∼3 nCi of the 5′-labeled DNA (20 μL total volume). The freshly oxidized $Ru^{IV}O^{2+}$ complex was immediately added to the DNA solution, and after 5 min, the reactions were quenched with 95% ethanol and lyophilized to dryness. The dried samples were then suspended in 0.7 M piperidine (60 μL) and incubated at 90 °C for 30 min. The reaction mixtures were lyophilized, washed with water (10 μL), lyophilized, and resuspended in the gel-loading buffer (5 μL) containing 80% formamide, 0.25% bromophenol blue, and 0.25% xylene cyanol FF.

In some instances it was necessary to remove the covalently bound metal complex from the DNA. Prior to piperidine treatment, the reaction samples were treated with 1 M KCN (60 μL) and dialyzed against distilled water for 3 h. The dialyzed samples were lyophilized and subjected to piperidine treatment, as described above.

The DNA fragments were analyzed using 20% polyacrylamide gel electrophoresis under denaturing conditions (7 M urea). Cleavage bands were visualized using Kodak Biomax MR single-emulsion film at −78 °C for 12−18 h. Quantitation of the extent of cleavage was performed by integration of the optical density as a function of the band area

(20) Sigman, D. S. *Biochemistry* **1990**, *29*, 9097−9105.
(21) Pratviel, G.; Bernadou, J.; Meunier, B. *Angew. Chem., Int. Ed. Engl.* **1995**, *34*, 746−769.
(22) Hecht, S. M. *Acc. Chem. Res.* **1986**, *19*, 83.
(23) Stubbe, J.; Kozarich, J. W. *Chem. Rev.* **1987**, *87*, 1107.
(24) Pyle, A. M.; Morii, T.; Barton, J. K. *J. Am. Chem. Soc.* **1990**, *112*, 9432.
(25) Sitlani, A.; Dupureur, C. M.; Barton, J. K. *J. Am. Chem. Soc.* **1993**, *115*, 12589−12560.
(26) Pyle, A. M.; Barton, J. K. *Prog. Inorg. Chem.* **1990**, *38*, 413.
(27) Terbrueggen, R. H.; Barton, J. K. *Biochemistry* **1995**, *34*, 8227−8234.
(28) Riordan, C. G.; Wei, P. *J. Am. Chem. Soc.* **1994**, *116*, 2189−2190.
(29) Pogozelski, W. K.; McNeese, T. J.; Tullius, T. D. *J. Am. Chem. Soc.* **1995**, *117*, 6428−6433.
(30) Breiner, K. M.; Daugherty, M. A.; Oas, T. G.; Thorp, H. H. *J. Am. Chem. Soc.* **1995**, *117*, 11673−11679.
(31) Burrows, C. J.; Rokita, S. E. *Acc. Chem. Res.* **1994**, *27*, 295−301.
(32) Takeuchi, K. J.; Thompson, M. S.; Pipes, D. W.; Meyer, T. J. *Inorg. Chem.* **1984**, *23*, 1845.
(33) Moyer, B. A.; Meyer, T. J. *Inorg. Chem.* **1981**, *20*, 436.
(34) Johnson, E. C.; Sullivan, B. P.; Salmon, D. J.; Adeyemi, S. A.; Meyer, T. J. *Inorg. Chem.* **1978**, *17*, 2211−2215.
(35) Maniatis, T.; Fritsch, E. F.; Sambrook, J. *Molecular Cloning: A Laboratory Manual*, 2nd ed.; Cold Spring Harbor Press: Plainview, NY, 1989.

using an Apple OneScanner and the Image program from the NIH. Quantitation was performed only when Gaussian peaks were observed and saturation of the film did not affect the results.

Results

Single-Stranded DNA. Cations bind to double-stranded DNA primarily because of the close proximity of anionic phosphate groups in the minor groove.[36] Single-stranded DNA does not present such organized anionic groups to bound cations and therefore exhibits a much lower affinity for bound cations. Further, the bases and sugars are much more accessible to exogenous agents, because protection of the activatable C−H bonds is provided by folding of the double helix.[37] As shown previously, $Ru^{IV}O^{2+}$ oxidation of d[5′-$A_1T_2A_3C_4G_5C_6A_7A_8$-$G_9G_{10}G_{11}C_{12}A_{13}T_{14}$], which is a random coil in solution, occurs with a guanine/sugar ratio that can be predicted from the rate constants for oxidation of mononucleotides.[9] Therefore, the cleavage pattern of single strands approximates the innate reactivity of the reactive functions toward the oxidant.

The ruthenium concentration dependence of the extent of cleavage of the random coil oligomer by $Ru(tpy)(bpy)O^{2+}$ was determined. The yield of cleavage at each site was quantitated by densitometry, and the sums of cleavage at G and at A, T, and C are shown in Figure 1A. Cleavage at A, T, and C occurs solely by sugar oxidation at 1′, while oxidation at G occurs primarily by oxidation of the guanine base.[8] The dependence of guanine cleavage on oxidant concentration bears a striking resemblence to kinetic traces that monitor the disappearance of $Ru^{IV}O^{2+}$ with time upon treatment with GMP.[9] Analysis of these traces shows that the delay in rapid reduction of the oxidant is caused by formation of an inner-sphere Ru^{III}−O−G adduct that is followed by a series of steps involving overoxidation of the adduct by additional equivalents of $Ru^{IV}O^{2+}$:

$$Ru^{IV}O^{2+} + GMP \rightarrow Ru^{III}-O-GMP \qquad (2)$$

$$Ru^{III}-O-GMP + Ru^{IV}O^{2+} \rightarrow \rightarrow Ru^{II}OH_2{}^{2+} + \text{oxidized guanine} \qquad (3)$$

The complete mechanism has been discussed in detail elsewhere.[9] The similarity of the concentration dependence of guanine oxidation in Figure 1A to the previously published decay curve at 398 nm, which is an isosbestic point at which only the disappearance of $Ru^{IV}O^{2+}$ is observed, suggests that adduct formation followed by oxidation of the adduct by a second equivalent of $Ru^{IV}O^{2+}$ contributes to the sigmoidal appearance of the curves in Figure 1, at least at the early concentration points.

Inspection of Figure 1 reveals that the guanine/sugar ratio varies with the concentration of oxidant. Therefore, quantitative comparison of the true ratio of rates must account for this dependence. For example, the guanine/sugar ratio is clearly different at 5 and 30 μM in Figure 1A. The curves for each individual nucleotide are subject to the same considerations. A rigorous kinetic analysis is not possible; however, we will now present a means of comparison that does account for the concentration dependence. The concentration dependence can be analyzed most simply if the first step is formation of an $Ru^{IV}O^{2+}$·DNA adduct (eq 4) that is probably an Ru^{III}−O−R complex. The second step that leads to formation of a piperdine-labile lesion is where $Ru^{IV}O^{2+}$ oxidizes the adduct (eq 5):

$$Ru^{IV}O^{2+} + DNA \rightarrow Ru^{IV}O^{2+}\cdot DNA \qquad (4)$$

$$Ru^{IV}O^{2+}\cdot DNA + Ru^{IV}O^{2+} \rightarrow \text{scission} \qquad (5)$$

If eq 5 is rate-limiting, then the rate = $k[Ru^{IV}O^{2+}][Ru^{IV}O^{2+}\cdot$DNA]. Applying the steady-state approximation to the $Ru^{IV}O^{2+}\cdot$DNA adduct provides a rate equation with $[Ru^{IV}O^{2+}]^2$ in the numerator. The squared dependence in the numerator can account for the parabolic appearance of the low-concentration points in Figure 1A. At high concentrations, saturation of the $[Ru^{IV}O^{2+}\cdot$DNA] adducts occurs. Replotting the data with $[RuO^{2+}]^2$ on the *x*-axis gives saturation plots, as shown in Figure 2. To assess the relative rates, we choose the slope of the low-concentration points in the saturation curve, as in determining second-order rate constants from Michaelis−Menten plots.

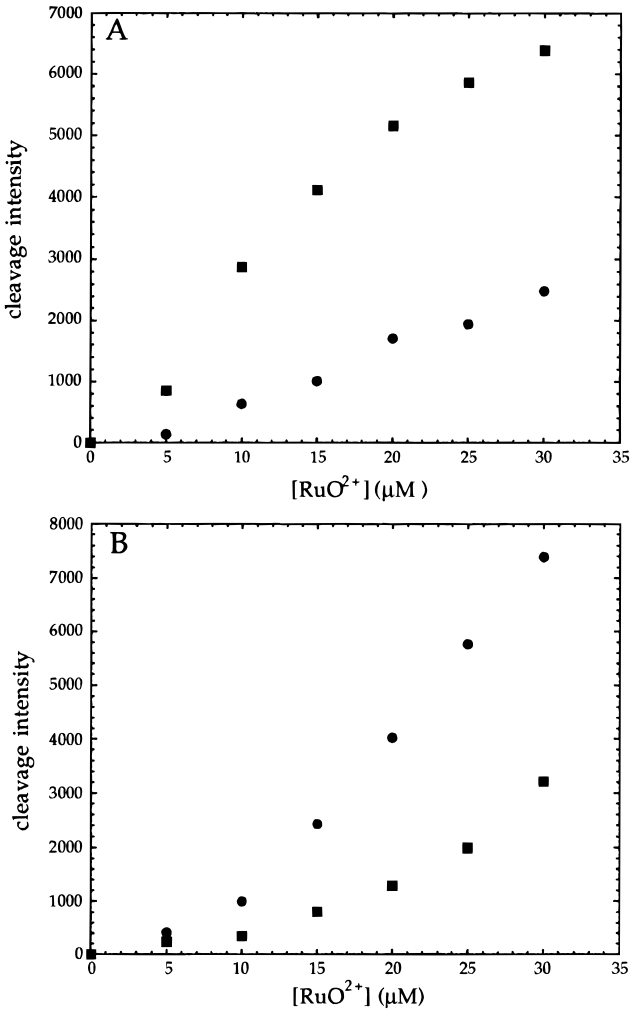

Figure 1. (A) Cleavage intensity (arbitrary units) of the random coil oligomer d[5′-$A_1T_2A_3C_4G_5C_6A_7A_8G_9G_{10}G_{11}C_{12}A_{13}T_{14}$] as a function of the concentration of $Ru(tpy)(bpy)O^{2+}$ for guanine oxidation (squares; G_5, G_9, G_{10}, and G_{11}) and sugar oxidation (circles; C_6, A_7, A_8, C_{12}, and A_{13}). (B) Cleavage intensity (arbitrary units) of the random coil oligomer d[5′-$A_1T_2A_3C_4G_5C_6A_7A_8G_9G_{10}G_{11}C_{12}A_{13}T_{14}$] hybridized to its complement as a function of the concentration of $Ru(tpy)(bpy)O^{2+}$ for guanine oxidation (circles; G_5, G_9, G_{10}, and G_{11}) and sugar oxidation (squares; C_6, A_7, A_8, C_{12}, and A_{13}).

The solid lines in Figure 2 show the fits for the linear regions of the $[RuO^{2+}]^2$ plots for the sum of all of the guanine sites and the A, T, and C (sugar) sites. The ratio of the guanine and sugar rates is 6.7 on a per nucleotide basis. We reported previously that simple quanitation of the total cleavage at guanine divided by the total cleavage at sugar gave a ratio of 7, in reasonable agreement with the ratio determined in Figure 2A.[9] We can now be confident that this ratio accounts for the

(36) Jayaram, B.; Sharp, K. A.; Honig, B. *Biopolymers* **1989**, *28*, 975−993.
(37) Johnston, D. H.; Glasgow, K. C.; Thorp, H. H. *J. Am. Chem. Soc.* **1995**, *117*, 8933−8938.

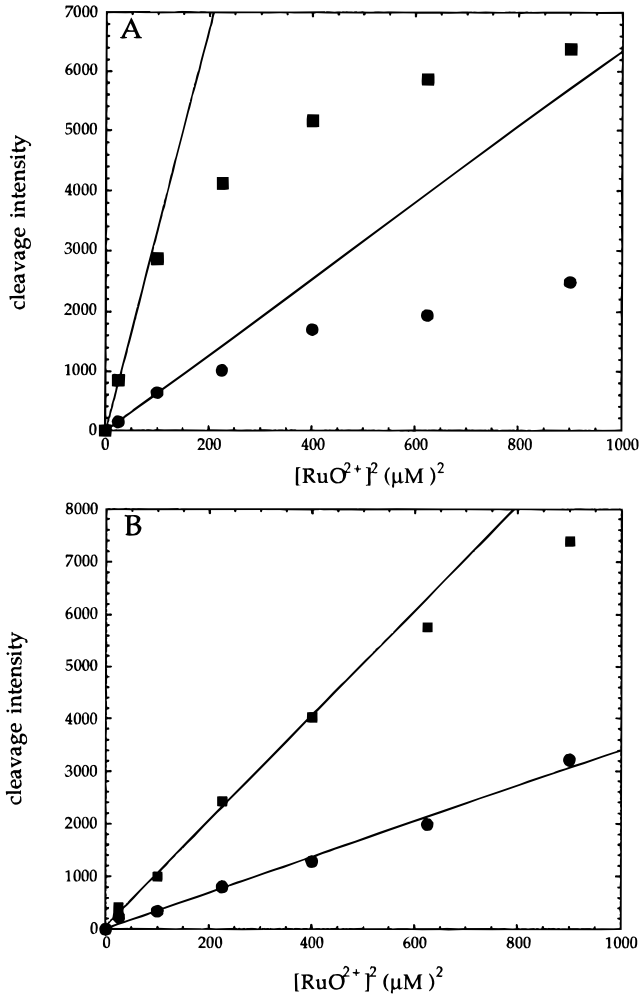

Figure 2. Data from Figure 1 replotted as a function of the square of the concentration of Ru(tpy)(bpy)O^{2+}. Solid lines are best linear fits to the low-concentration points.

dependence on the concentration of RuO^{2+}, which will be important in the case where very different reactivities are observed within the same sequence. Rates were also determined similarly for each individual site, and the relative values are shown in Table 2. The reactivities of the individual sites are given relative to G_{10}, which was the most reactive. The slopes for the guanine sites follow the order $G_{10} > G_{11} > G_5 > G_9$, while the sugar sites follow the order $C_{12} > A_{13} > C_6 > A_8 > A_7$.

The concentration dependence for cleavage of the same labeled random coil hybridized to its complement was also determined. Qualitatively, higher concentrations of $Ru^{IV}O^{2+}$ were required to observe comparable extents of cleavage, as we have published elsewhere.[8] Since the binding affinity is higher for the duplex, this effect likely arises from greater difficulty in accessing the site of oxidation. The cleavage yields as a function of $[Ru^{IV}O^{2+}]$ are shown in Figure 1B, and the rates were determined in the same manner as for the single strand (Figure 2B, Table 1). This analysis gives a guanine/sugar ratio of 4.1 on a per nucleotide basis, considerably lower than that in the single strand.

As with the single strand, the rate of cleavage at each individual site was also evaluated (Table 2). The lower ratio of guanine oxidation to sugar oxidation is apparent in the relative reactivities (note that the absolute magnitudes for the single strand and duplex are not comparable). A striking result is that the relative reactivities of the guanines ($G_{10} > G_{11} > G_5 > G_9$) and the sugars ($C_{12} > A_{13} > C_6 > A_8 > A_7$) are the same in both the single and double strands. Formation of the duplex therefore lowers the overall reactivity and decreases the guanine-to-sugar ratio. However, the secondary structure apparently does not influence the selectivity among different guanines or among different sugars, implying that these selectivities arise from sequence-specific chemical reactivities.

Table 1. Kinetic Parameters for Guanine and Sugar Oxidation of Single-Strand and Duplex Forms of d[5′-$A_1T_2A_3C_4G_5C_6A_7A_8G_9G_{10}G_{11}C_{12}A_{13}T_{14}$]

	slope	
	single-strand	duplex
guanine[a]	34	10
sugar[b]	6.4	3.2

[a] Sum of cleavage rates at G_5, G_9, G_{10}, and G_{11}. [b] Sum of cleavage rates at C_6, C_7, C_8, C_{12}, and A_{13}.

Table 2. Relative Cleavage Rates at Individual Sites for Single-Strand and Duplex Forms of d[5′-$A_1T_2A_3C_4G_5C_6A_7A_8G_9G_{10}G_{11}C_{12}A_{13}T_{14}$][a]

	G5	C6	A7	A8	G9	G10	G11	C12	A13
ss	60	10	3	3	21	100	70	15	12
ds	56	14	8	13	39	100	66	29	21

[a] Rates were obtained from fitting of the linear region of plots of cleavage versus $[RuO^{2+}]^2$ at each site as shown in Figure 2 and are relative to G_{10} for each case.

DNA Hairpin Oxidation. Since the behavior of the complex was different with single- and double-stranded DNA, we chose to study oxidation of DNA hairpins. The hairpin structure allows the effects of secondary structure to be assessed directly on the same oligomer, where comparison between different gels or different samples is not a complication. The structure of the hairpin d[5′-$C_1G_2C_3G_4$**$T_5T_6G_7T_8T_9$**$C_{10}G_{11}C_{12}G_{13}$] (loop residues in bold) has been characterized by two-dimensional NMR.[38] The structure was appealing for these studies because the loop guanine (G_7) is highly solvent accessible and sits at the top of the hairpin stack where it is completely exposed to the solution. Results of cleavage of this hairpin by Ru(tpy)(bpy)O^{2+} are shown in Figure 3. Piperidine-labile cleavages are observed to some extent at nearly every site in the hairpin; however, the cleavage at G_7 is significantly more efficient than that at any other site. In particular, the cleavage of the stem guanines (G_{11} and G_{13}) is not significantly enhanced compared to the sugar sites, consistent with the lower guanine/sugar ratio seen in the double strand compared to the single strand in Table 1.

The structure of the loop region of the DNA hairpin d[5′-$A_1T_2C_3C_4T_5A_6$**$T_7T_8T_9$-A_{10}**$T_{11}A_{12}G_{13}G_{14}A_{15}$] has also been studied by 2-D NMR.[39] In the tetraloop, the thymine base from T_8 is folded out of the loop into the minor groove, and there is a T_7-A_{10} Hoogsteen base pair that is stacked with T_9. This hairpin provides an excellent complement to the TTGTT hairpin from Figure 3, because there are no guanines in the loop region. Cleavage in the loop region therefore occurs only by sugar cleavage and can be considered solely on the accessibility and reactivity of the 1′ hydrogens. The results of oxidation of the TTTA hairpin are shown in Figure 4. Among the loop residues, cleavage at A_{10} and T_8 is enhanced compared to the stem sugar residues, cleavage at T_7 is about the same as the stem sugars, and cleavage at T_9 is conspicuously absent.

Inspection of the structure of the loop region of the TTTA hairpin[31] provides an explanation for the $A_{10} \sim T_8 > T_7 > T_9$

(38) Williamson, J. R.; Boxer, S. G. *Biochemistry* **1989**, *28*, 2819−2831.
(39) Blommers, M. J. J.; Van de Ven, F. J. M.; Van der Marel, G. A.; van Boom, J. H.; Hilbers, C. W. *Eur. J. Biochem.* **1991**, *201*, 33−51.

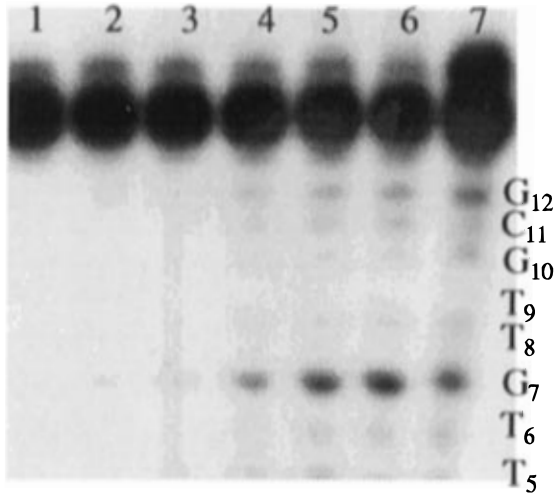

Figure 3. Autoradiogram of a polyacrylamide gel showing the results of the oxidation of the 5′-^{32}P-labeled hairpin d[5′-CGCG**TTGT-T**CGCG] (where the bold residues represent those in the hairpin loop) by Ru(tpy)(bpy)O^{2+}. The DNA concentration was 5 μM, and all samples were treated with piperidine (90 °C, 30 min). Lane 1, DNA alone; lane 2, [$Ru^{IV}O^{2+}$] = 5 μM; Lane 3, [$Ru^{IV}O^{2+}$] = 10 μM; lane 4, [$Ru^{IV}O^{2+}$] = 25 μM; lane 5, [$Ru^{IV}O^{2+}$] = 35 μM; lane 6, [$Ru^{IV}O^{2+}$] = 50 μM; lane 7, G + A reaction.

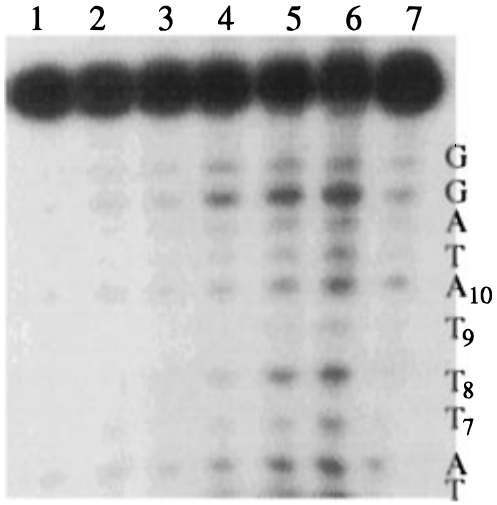

Figure 4. Autoradiogram of a polyacrylamide gel showing the results of the oxidation of the 5′-^{32}P-labeled hairpin DNA d[5′-ATCCTA**TT-TA**TAGGAT] by Ru(tpy)(bpy)O^{2+}. The DNA concentration was 5 μM, and all samples were treated with piperidine (90 °C, 30 min). Lane 1, DNA alone; lane 2, [$Ru^{IV}O^{2+}$] = 5 μM; lane 3, [$Ru^{IV}O^{2+}$] = 10 μM; lane 4, [$Ru^{IV}O^{2+}$] = 25 μM; lane 5, [$Ru^{IV}O^{2+}$] = 35 μM; lane 6, [$Ru^{IV}O^{2+}$] = 50 μM; lane 7, G + A reaction.

cleavage pattern. Folding of T_8 into the minor groove forces the sugar to rotate out of the interior of the loop and exposes the 1′ hydrogen to the solvent. Formation of the A_{10}−T_7 Hoogsteen pair requires that the A_{10} sugar rotates about the stem axis and adopts the *high-syn* conformation about the glycosidic bond, also directing the 1′ hydrogen toward the solvent. The sugar of the T_9 residue is turned out such that the 2′ and 3′ hydrogens are oriented parallel to the stem axis toward the solution and the 1′ hydrogen is turned toward the loop interior. The thymine of T_7 is stacked on top of the A_6•T_{11} base pair of the stem, so the sugar of T_7 is indistunguishable from that of the regular B-DNA conformation. These configurations are all consistent with the cleavage pattern, because cleavage of A_{10} and T_8 is enhanced compared to the stem, cleavage at T_9 is significantly less than in the stem, and cleavage at T_7 is about the same. Importantly, the cleavage intensities at A_{10}, T_8, and T_9 are significantly different from the stem intensities, and these three sugars exhibit sugar conformations that are different from those of regular B-DNA. On the other hand, the sugar conformation of T_7 is the same as that in B-DNA and exhibits the similar cleavage intensity to the stem sugar sites.

Steric Effects. Having shown that structurally characterized hairpins provide predictable cleavage patterns, we applied these reagents to a hairpin of unknown structure, d[5′-$T_1T_2C_3A_4A_5$-**$C_6A_7G_8T_9G_{10}T_{11}$**$T_{12}T_{13}G_{14}A_{15}A_{16}$]. The design of this hairpin was based on the RNA hairpin from the iron recongition element (IRE) mRNA for ferritin,[40−42] although because of the different stacking in DNA and RNA hairpin loops,[43,44] this hairpin is not necessarily a model for the IRE. Cleavage of this hairpin by Ru(tpy)(bpy)O^{2+} has been described elsewhere[9,45] and proceeds with the strongest site at the G_8 loop site, which is more reactive than G_{10}, which is much more reactive than the stem G_{14}. Formation of the hairpin structure was confirmed by non-denaturing electrophoresis and thermal denaturation.

The oxidation of GMP by Ru(tpy)(bpy)O^{2+} occurs through a bound Ru^{III}−O−GMP adduct,[9] as evidenced by global analysis of stopped-flow traces. At the moment, the specific site (or sites) in guanine that is attacked is unknown. A small amount of 8-oxo-G has been detected in oxidations of 9-ethylguanine, implying that at least some of the oxidation proceeds through a Ru^{III}−O−C8 intermediate (**A**).[9] We reasoned that this

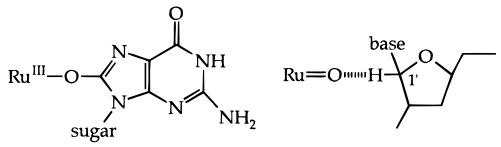

A **B**

pathway would be more sensitive to the solvent accessibility of the oxo group in $Ru^{IV}O^{2+}$ than the sugar reaction, where the sugar hydrogen is abstracted across some finite distance (**B**). The smaller guanine-to-sugar ratio seen in the duplex compared to the single strand in Table 1 implies that the guanine pathway is more sensitive to steric control than the sugar pathway, as does the greater reactivity of the loop guanines in the hairpins.

The cleavage of the hairpin has been examined with a series of three $Ru^{IV}O^{2+}$ complexes with differing oxo group accessibilities. In all three complexes, at least two of the sites adjacent to the oxo ligand are occupied by pyridyl groups oriented perpindicular to the Ru═O bond (Figure 5). The least sterically hindered complex is *cis*-Ru(bpy)$_2$(OH_2)O^{2+} (**1**) where one site *cis* to the oxo ligand is ligated only by a small aqua ligand and the other site by a pyridine parallel to the Ru═O bond. The Ru(tpy)(bpy)O^{2+} (**2**) complex is more hindered, because one site is still next to a pyridine that is parallel to the Ru═O bond while the other site is occupied by a perpindicular pyridine. Finally, the complex *cis*-Ru(bpy)$_2$(py)O^{2+} (**3**) is the most hindered, because two sites adjacent to the oxo ligand are occupied by parallel pyridyl moieties.

Qualitatively, the cleavage patterns for all three complexes are similar. Examination of the cleavage intensities reveals the pattern **1** ≫ **2** > **3** for guanine oxidation, as expected on the basis of the solvent accessibilities. A histogram showing the

(40) Klausner, R. D.; Rouault, T. A.; Harford, J. B. *Cell* **1993**, *72*, 19−28.
(41) Theil, E. C. *Biochem. J.* **1994**, *304*, 1−11.
(42) O'Halloran, T. V. *Science* **1993**, *261*, 715−725.
(43) Erie, D. A.; Suri, A. K.; Breslauer, K. J.; Jones, R. A.; Olson, W. K. *Biochemistry* **1993**, *32*, 436−454.
(44) Haasnoot, C. A. G.; Hilbers, C. W.; van der Marel, G. A.; van Boom, J. H.; Singh, U. C.; Pattabiraman, N.; Kollman, P. A. *J. Biomol. Struct. Dyn.* **1986**, *3*, 843−857.
(45) Cheng, C.-C.; Thorp, H. H. Unpublished results.

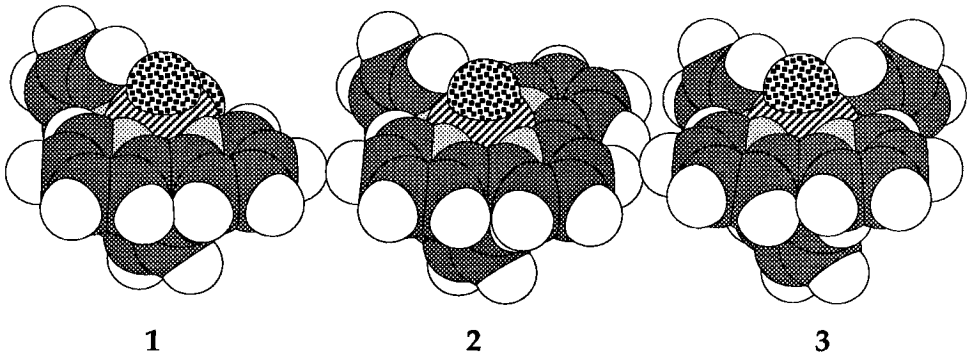

Figure 5. Space-filling models of complexes $Ru(bpy)_2(OH_2)O^{2+}$ (**1**), $Ru(tpy)(bpy)O^{2+}$ (**2**), and $Ru(bpy)_2(py)O^{2+}$ (**3**).

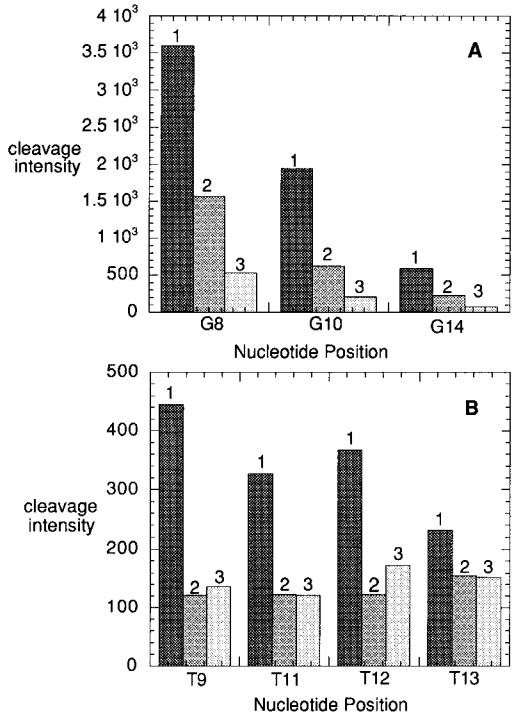

Figure 6. (A) Histogram showing the yields of guanine oxidation in d[5′-$T_1T_2C_3A_4A_5$**C$_6$A$_7$G$_8$T$_9$G$_{10}$T$_{11}$**$T_{12}T_{13}G_{14}A_{15}A_{16}$] for complexes **1**−**3**. (B) Histogram showing the yields of thymine oxidation in the same oligomer for complexes **1**−**3**.

results for guanine oxidation is shown in Figure 6A. For all four complexes, G_8 is more reactive than G_{10}, which is more reactive than G_{14}. This same pattern is observed in the natural IRE mRNA.[46] Further, the relative intensities for all four complexes are the same for each site ($G_8 > G_{10} > G_{14}$), showing that solvent accessibility is important in guanine oxidation regardless of the secondary structure. This result parallels the observation that the relative intensities of all four guanines in Table 2 are the same in the single strand and duplex.

The cleavage intensities for oxidation of thymidine sugars is shown in Figure 6B. For the loop and stem-loop junction sites (T_9, T_{11}, and T_{12}), the pattern **1** > **2** ∼ **3** is observed. However, the intensities for **1**, **2**, and **3** are all about the same in the stem site T_{13}. Therefore, in the stem and stem−loop sites where the sugars are more accessible, the dramatic difference in oxo group accessibility for **1** compared to the others is still important, although not as important as in guanine oxidation. However, in the duplex site, where the reaction rate is slow, the differences in accessiblity are no longer important.

Discussion

The squared dependence of the low-concentration points in Figure 1 is consistent with kinetic studies on GMP oxidation that have been discussed in detail elsewhere.[9] These studies imply the formation of a covalent adduct between $Ru(tpy)(bpy)O^{2+}$ and guanine, and the spectrum of the adduct is consistent with a Ru(III) alkoxide complex. Small amounts of 8-oxoguanine have been detected in the reaction of ethylguanine with $Ru(tpy)(bpy)O^{2+}$;[9] the low yield could result either from the involvement of multiple pathways or from overoxidation of the 8-oxoguanine product by free $Ru(tpy)(bpy)O^{2+}$. New experiments in our laboratory indicate a kinetic isotope effect for deuteration of the C8 position.[47] Recent studies have demonstrated the formation of a novel covalent adduct between guanine and a polypyridyl ligand during guanine oxidation by simple electron transfer,[48] which is probably not relevant to the adduct formed with $Ru(tpy)(bpy)O^{2+}$. The relative reactivities (Table 1) indicate that formation of the covalent adduct is more facile in the single strand compared to the duplex, where steric accomodation of the bulky metal complex is apparently problematic.

The oxidation of mononucleotides containing adenine, thymine, and cytosine did not provide evidence for the participation of a $Ru^{III}-O-R$ covalent intermediate,[9] yet the data in Figure 2 clearly indicate a squared dependence on $[Ru^{IV}O]$ at low concentrations. In the mononucleotide kinetics studies, the sugar oxidation reactions proceeded through a noncovalent electrostatic intermediate:

$$Ru^{IV}O^{2+} + AMP \rightleftharpoons Ru^{IV}O^{2+}\cdot AMP \quad (6)$$

$$Ru^{IV}O^{2+}\cdot AMP \rightarrow Ru^{II}OH_2{}^{2+} + \text{products} \quad (7)$$

where AMP is adenosine-5′-monophosphate; similar mechanisms were observed with cytosine and thymine nucleotides. The noncovalent adduct formed in eq 6 is different from that formed with GMP (eq 2) in the following ways: eq 6 must be treated as a reversible equilibrium to fit the kinetic data, higher ionic strength disfavors eq 6, replacement of AMP with ADP increases the equilibrium constant for eq 6, and the optical spectrum of the adduct is indistinguishable from that of authentic $Ru^{IV}O^{2+}$. In contrast, Meyer et al. have observed $Ru^{III}-O-R$ covalent intermediates in the oxidation of cyclohexene and alcohols that resemble the 1′ C−H activation in nucleotides.[49] It is possible that the involvement of eq 6 prevents observation of the covalent adduct. The results in Figure 2 therefore provide the first evidence that such adducts are important in sugar oxidation.

(46) Thorp, H. H.; McKenzie, R. A.; Lin, P.-N.; Walden, W. E.; Theil, E. C. *Inorg. Chem.* **1996**, *35*, 2773−2779.
(47) Farrer, B.; Thorp, H. H. Unpublished results.
(48) Jacquet, L.; Kelly, J. M.; Kirsch-De Mesmaeker, A. *J. Chem. Soc., Chem. Commun.* **1995**, 913−914.
(49) Stultz, L. K.; Binstead, R. A.; Reynolds, M. S.; Meyer, T. J. *J. Am. Chem. Soc.* **1995**, *117*, 2520−2532.

The existence of the $Ru^{III}-O-R$ covalent adduct can therefore be exploited to tune the ratio of oxidation of guanine to sugar. The oxidation of the single strand and duplex of the same oligomer show that the guanine-to-sugar ratio is nearly twice as high in the single strand, which could arise simply because the guanine is buried more deeply in the helix than the sugar phosphate backbone. The ability of the double helix to protect guanine from oxidation by both inner-sphere and outer-sphere pathways has been documented.[31,37,50] However, if the guanine reaction is also more sterically demanding intrinsically compared to the sugar reaction (i.e., **A** vs **B**), the sensitivity of the guanine-to-sugar ratio will be amplified. The results for the sterically differentiated complexes (Figure 5) emphasize this point; the guanine pathway is susceptible to steric attenuation while the reactivity at T_{13} is the same for **1**, **2**, and **3**.

A startling finding, apparent in Table 2, is that the relative reactivities of the different guanines are the same in the single and double strands. Likewise, the relative reactivities of the sugars are also the same in both. The only effects of hybridizing the random coil to its complement are a decrease in total reactivity and a decrease in the guanine-to-sugar ratio. This result implies that the relative reactivities result at least partly from sequence-dependent changes in the innate reactivity of the individual sites toward the oxidant. As discussed elsewhere,[1,8] these differences could arise either because of different activation parameters for C−H oxidation at individual sites on the oligomer or because of sequence-dependent changes in the rates of competing reactions, such as self-oxidation or dissociation.

Finally, the hairpin results show that the trends apparent for the single and double strands can be extrapolated to hybrid structures. The loop regions are more reactive than the stems, and this effect is more pronounced for guanine, as expected. The combined results therefore implicate a sterically more demanding pathway to guanine oxidation. Extension of these principles to more complicated and physiologically relevant polymers can be envisioned.

Acknowledgment. We thank Professor Gary Pielak for useful discussions. We thank the National Science Foundation for support. H.H.T. acknowledges the support of a Camille Dreyfus Teacher-Scholar Award.

IC9515517

(50) Chen, X.; Burrows, C. J.; Rokita, S. E. *J. Am. Chem. Soc.* **1992**, *114*, 322.